Journal of Coordination Chemistry

ISSN: 0095-8972 (Print) 1029-0389 (Online) Journal homepage: http://www.tandfonline.com/loi/gcoo20

The syntheses, crystal structure, thermal analysis, and anticancer activities of novel dipicolinate complexes

Nazlı Uzun, Alper Tolga Çolak, Fatih Mehmet Emen, Gorkem Kismali, Ogunc Meral, Merve Alpay, Gülbanu Koyundereli Çılgı & Ertan Şahin

To cite this article: Nazlı Uzun, Alper Tolga Çolak, Fatih Mehmet Emen, Gorkem Kismali, Ogunc Meral, Merve Alpay, Gülbanu Koyundereli Çılgı & Ertan Şahin (2015) The syntheses, crystal structure, thermal analysis, and anticancer activities of novel dipicolinate complexes, Journal of Coordination Chemistry, 68:6, 949-967, DOI: 10.1080/00958972.2014.1003371

To link to this article: http://dx.doi.org/10.1080/00958972.2014.1003371

Journal of Coordination Chemistry, 2015
Vol. 68, No. 6, 949–967, http://dx.doi.org/10.1080/00958972.2014.1003371

The syntheses, crystal structure, thermal analysis, and anticancer activities of novel dipicolinate complexes

NAZLI UZUN†, ALPER TOLGA ÇOLAK*†, FATIH MEHMET EMEN‡, GORKEM KISMALI§, OGUNC MERAL§, MERVE ALPAY§, GÜLBANU KOYUNDERELI ÇILGI¶ and ERTAN ŞAHIN‖

†Faculty of Arts and Sciences, Department of Chemistry, Dumlupınar University, Kütahya, Turkey
‡Faculty of Arts and Sciences, Department of Chemistry, Mehmet Akif Ersoy University, Burdur, Turkey
§Faculty of Veterinary Medicine, Department of Biochemistry, Ankara University, Ankara, Turkey
¶Faculty of Technology, Department of Material Science and Engineering, Pamukkale University, Denizli, Turkey
‖Science Faculty, Department of Chemistry, Atatürk University, Erzurum, Turkey

(*Received 3 September 2014; accepted 1 December 2014*)

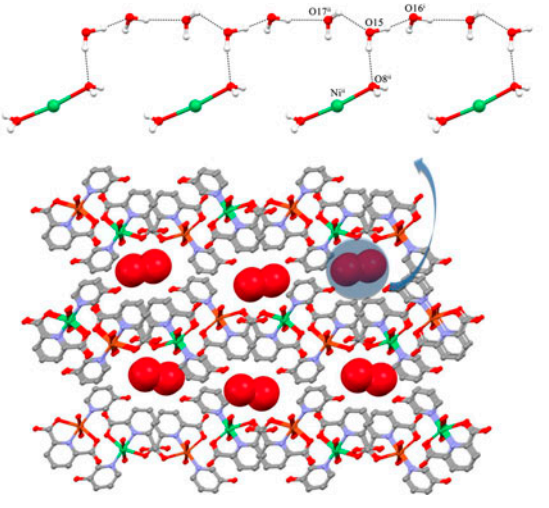

$[Cu(pydc)(eim)_3]\cdot H_2O$ (**1**), $[Cu(pydc)(4hp)(H_2O)]$ (**2**), and $[Ni(pydc)(3hp)(H_2O)_2][Cu(pydc)(3hp)(H_2O)_2]\cdot 3H_2O$ (**3**) (H_2pydc = 2,6-pyridinedicarboxylic acid or dipicolinic acid, eim = 2-ethylimidazole, 4h*p* = 4-hydroxypyridine, 3h*p* = 3-hydroxypyridine) were synthesized and characterized by elemental analysis, spectroscopic measurements (UV–vis and IR spectra), and single-crystal X-ray diffraction. Crystal analysis revealed that the complexes extended to 3-D supramolecular networks through intermolecular H-bonding and molecular interactions between the ligand moieties and water molecules. The thermal stabilities of complexes are investigated by thermogravimetry, differential thermogravimetry, and differential thermal analysis techniques. The effects of complexes on the

*Corresponding author. Email: tolga.colak@dpu.edu.tr

proliferation of HT-1080 fibrosarcoma cells were investigated using the quick cell proliferation assay. The cell viability changes were found to depend on the concentrations and type of complex.

Keywords: 2,6-Pyridinedicarboxylate; Crystal structure; Thermal analysis; Anticancer activities

1. Introduction

Natural and synthetic chemical complexes have been synthesized to treat cancer. Drugs obtained from these complexes have dangerous side effects and suffer from drug resistance. There have been a number of studies on substituting these drugs with favorable alternatives and numerous metal complexes have been examined for their anticancer activities [1–3]. Metal-based complexes containing of platinum, palladium, titanium, copper, ruthenium, tin, and rhodium have been reported to have promising chemotherapeutic potential [4]. Of the transition metal complexes, Cu(II) complexes are the best alternatives to cisplatin [5]. Copper takes on an important role in endogenous oxidative DNA injury associated with aging and cancer [6]. Copper is an essential trace element required for enzymes and animal tissues in biological systems in both the +1/+2 valence states; hence, it is involved in redox metalloenzymes and in oxygenation and oxygen-carrying proteins [7]. The binding of copper ions to specific sites can modify the conformational structures of proteins, polynucleotides, DNA, and bio-membranes [8]. The binding of Cu to DNA occurs [9]. Copper (II) carboxylates are more potent than their parent acids [10–13]. Their cancer activities are improved in the presence of auxiliary nitrogen–oxygen donor ligands [14–17]. Pyridine-2,6-dicarboxylic acid (H_2pydc, also known as dipicolinic acid) possesses diverse function portions and can form bridging hydrogen bonds with the potential for self-assembly [18–26]. H_2pydc is a good hydrogen-bond acceptor and can form strong hydrogen bonds, and hydrogen-bond networks with H-donors [27–29]. H_2pydc has been studied extensively as Lewis base and it has hundreds of complexes [30–40]. However, these studies are mostly concerned with structural characterization. Although there are hundreds of studies about this valuable ligand in the literature, the number of studies on cancer activity of these complexes is limited [41, 42]. In the present study, we have described the synthesis, spectroscopic and thermal analysis, crystal structures, and anticancer activities of $[Cu(pydc)(eim)_3]\cdot H_2O$ (**1**), $[Cu(pydc)(4hp)(H_2O)]$ (**2**) and $[Ni(pydc)(3hp)(H_2O)_2][Cu(pydc)(3hp)(H_2O)_2]\cdot 3H_2O$ **(3)**.

2. Experimental studies

2.1. *Materials and measurements*

All chemicals and solvents used for syntheses were of reagent grade. Pyridine-2,6-dicarboxylic acid, 3-hydroxypyridine, 4-hydroxypyridine, C_2H_5OH, $Cu(CH_3COO)_2\cdot H_2O$, and $Ni(CH_3COO)_2\cdot 4H_2O$ (Aldrich) were used as received. Elemental analyses (C, H, and N) were performed using a Vario EL III CHNS elemental analyser. Magnetic susceptibility measurements were performed at room temperature using a Sherwood Scientific MK1 model Gouy magnetic balance. UV–vis spectra were obtained in DMSO (10^{-3} M/L) of the complexes with a Shimadzu Pharmaspec UV-1700 spectrometer from 1000 to 190 nm. FT-IR spectra were recorded from 4000 to 400 cm^{-1} with a Bruker Optics Vertex 70 FT-IR spectrometer using KBr pellets. A Perkin Elmer DV 4300 inductively coupled plasma–optical emission spectrophotometer was used to analyze copper(II) and nickel(II) in the digested samples.

All of the thermogravimetry (TG), differential thermogravimetry (DTG), and differential thermal analysis (DTA) curves were obtained simultaneously by using a Shimadzu DTG-60H Thermal Analyser. The measurements were carried out in flowing nitrogen (100 mL/min) and the temperature ranged from 300 to 1000 K in an alumina crucible. Highly sintered Al_2O_3 was used as the reference material. The selection of lower heating rates (β) is very important to distinguish each reaction and to determine the initial and final temperatures of the reactions. Moreover, lower heating rates allow for completion of the reaction and full removal of the volatile products from the solid material. Therefore, lower heating rates (5, 7, and 10 °C/min) were tested and were found as optimum heating rates in terms of both the time and kinetic analyses. The sample mass (w_o) ranged between 4 and 5 mg. To calibrate the temperature, the melting points of indium and tin were used, which were provided by Shimadzu.

2.2. *Crystallographic analyses*

For determination of the crystal structure, single-crystals of the Cu(II)/Ni(II) complexes **1**, **2**, and **3** were used for data collection on a four-circle Rigaku R-AXIS RAPID-S diffractometer (equipped with a two-dimensional area IP detector). The graphite-monochromated Mo K_α radiation (λ = 0.71073 Å) and oscillation scans technique with $\Delta\omega = 5°$ for one image were used for data collection. The lattice parameters were determined by least-squares on the basis of all reflections with $F^2 > 2\sigma(F^2)$. Integration of the intensities, correction for Lorentz and polarization effects, and cell refinement were performed using the Crystal Clear (Rigaku/MSC Inc., 2005) software [43]. The structures were solved by direct methods using SHELXS-97 [44] and refined by a full-matrix least-squares procedure using SHELXL-97 [44]. Hydrogens were positioned geometrically and refined using a riding model. The final difference Fourier maps showed no peaks of chemical significance. Crystal data and additional data collection parameters and refinement details are presented in table S1 (see online supplemental material at http://dx.doi.org/10.1080/00958972.2014.1003371).

2.3. *Biological evaluation*

2.3.1. Cell culture. The human fibrosarcoma HT-1080 was purchased from ATCC (Wesel, Germany, Cat. CCL-121). HT-1080 cells were maintained in DMEM-F12 with 584 mg/L of L-Glutamine and HEPES (Irvine Scientific, Santa Ana, California, USA) containing 10% fetal bovine serum (Irvine Scientific, Santa Ana, California, USA) and 50 µg/mL gentamycin sulfate solution (Irvine Scientific, Santa Ana, California, USA). Cells were grown in 75 cm^2 vented cap flasks (BD Falcon, Rockville, MD, USA) in a humidified (5% CO_2) incubator at 37 °C. The medium was changed every two days. Cells were sub-cultured at a ratio of 1 : 4 with trypsin-EDTA solution (Irvine Scientific, Santa Ana, California, USA).

2.3.2. Cell proliferation/viability assay. Cells were counted using a Neubauer hemocytometer. To study the viability, fibrosarcoma cells were seeded in 96-well flat bottom cell culture plates (Greiner Bio One, Frickenhausen, Germany) at a density of 1×10^5 cells/well in 100 µL of culture medium. The cells were incubated in plates for 24 h before the experiment to enable attachment. Dead or unattached cells were removed by washing twice with phosphate buffered saline (Irvine Scientific, Santa Ana, California, USA) before all assays.

A colorimetric assay was used for the quantification of cell proliferation and cell viability, based on the cleavage of the tetrazolium salt WST-1 to formazan by cellular mitochondrial dehydrogenases (The Quick Cell Proliferation Assay Kit, Biovision, San Francisco, USA). The formazan dye produced by viable cells was quantified spectrophotometrically. Assays were performed according to the manufacturer's protocol. The cells were briefly seeded in 96-well microtiter plates in a medium containing final volume of 100 μL, and incubated under normal cell culture conditions for 24 h before each experiment. WST-1/Electrocoupling solution (10 μL/well) was added in all control and experiment cell groups. Following 1 h incubation, absorbance values were measured at 420–650 nm in a microtiter plate reader. The results were presented as % cell viability. Each experiment was done in triplicate.

2.3.3. DAPI nuclear staining. The blue-fluorescent 4,6-diamidino-2-phenylindole (DAPI) nucleic acid stain preferentially stains dsDNA. It appears to associate with AT clusters in the minor groove. The binding of DAPI to dsDNA produces a ~20-fold fluorescence enhancement, apparently due to the displacement of water molecules from both DAPI and the minor groove. Changes in cell morphology and characteristics of apoptosis were examined by fluorescence microscopy of DAPI-stained cells (Leica DMI 4000, Wetzlar, Germany). For morphological observations, 1×10^6 cells/well in 1 mL of culture medium was seeded in 2-well chamber slides (Lab-Tek II Chamber Slide, Nunc, Rochester, New York, USA). The same sub-cultured cells were used in each experiment to prevent any effect of cell age on the experiment (8th passages). The adherent monolayer cells were grown in two-well chamber slides, and washed twice with PBS. The DAPI stain (Gerbu, Wieblingen, Germany) was prepared at a 1 : 1000 dilution in water for injection (WFI) grade water and then added in the cells so that they were completely covered. Incubation was performed for 15 min at room temperature in the dark. At the end of the incubation period, the DAPI solution was aspirated, then the slides were washed once with PBS. The apoptotic nuclei (intensely stained, fragmented nuclei, and condensed chromatin) were examined using a fluorescence microscope (Leica DMI 4000, Wetzlar, Germany) with 340–380 nm excitations.

2.3.4. Assessment of cell injury. Any injury of the fibrosarcoma cells was quantified by measuring the release of Lactate Dehydrogenase (LDH) from lysed cells into the bathing medium. The cells (1×10^5 cells/well) were placed in 96-well plates and incubated with the complexes for 24 h. Concentrations of supernatant LDH levels were determined using a commercially available colorimetric assay kit (TML Medical, Ankara, Turkey). A Clinical Chemistry Analyser (ERBA XL 600, Meinheim, Germany) was used for the analysis. Total LDH release corresponding to complete fibrosarcoma death was determined for each experiment. Glucose levels were also determined using a commercially available colorimetric assay kit from TML Medical (Turkey). The total glucose release corresponding to complete HT-1080 death was determined.

2.4. *Preparation of complexes*

A solution of H_2pydc (1.0 mM, 0.167 g) in water (20 mL) was added dropwise, and stirred at room temperature, to solutions of $Cu(CH_3COO)_2{\cdot}H_2O$ (1.0 mM, 0.20 g), Ni

$(CH_3COO)_2{\cdot}4H_2O$ (1.0 mM, 0.25 g) (only for **3**) and KOH (2.0 mM, 0.11 g) in 20, 20, and 10 mL water, respectively. The solution immediately became a suspension and was stirred for 5 h at reflux. Then, the 2-ethylimidazole (3.0 mM, 0.29 g) for **1** or 4-hydroxypyridine (3 mM, 0.28 g) for **2**, or 3-hydroxypyridine (3.0 mM, 0.28 g) for **3** in water (20 mL) was added dropwise to this suspension. The clear solution was stirred for 4 h at 80 °C and then cooled to room temperature. After a month, crystals formed, were filtered and washed with 10 mL of cold ethanol and dried in air. *Analytical Data*: $C_{22}H_{29}CuN_7O_5$ for **1** (535.1 g/M) = Calcd C 49.38, H 5.46, N 18.32, Cu 11.88; found C 49.15, H 5.28, N 17.91, Cu 11.36. Yield 44%, *Analytical Data*: $C_{12}H_{10}CuN_2O_6$ for **2** (341.8 g/M) = Calcd C 42.17, H 2.95, N 8.20, Cu 18.59; found C 42.64, H 3.10, N 8.45, Cu 18.84. Yield 68%. *Analytical Data*: $C_{24}H_{30}CuN_4NiO_{17}$ for **3** (768.8 g/M) = Calcd C 37.50, H 3.93, N 7.29, Cu 8.27, Ni 7.63; found C 37.25, H 3.22, N 7.03, Cu 8.61, Ni 7.85, Yield 34%,

3. Results and discussion

3.1. *UV–vis spectra, FT-IR spectra, and magnetic susceptibilities*

The electronic spectrum of **1** in water exhibits an absorption at 755 ($\varepsilon = 19$ L M^{-1} cm^{-1}) which can be attributed to $^2E_g \rightarrow {}^2T_{2g}$ transitions. The 794 nm value was attributed to d_{xz}, $d_{yz} \rightarrow d_{x2-y2}$ ($a_1 \rightarrow b_1$) transition, which lies within one broad envelope for **2**. We expected $^3A_{2g} \rightarrow {}^3T_{1g}$ (F) and $^2E_g \rightarrow {}^2T_{2g}$ transitions for Ni(II) and Cu(II) ions, respectively, in 3. However, this appears as a single broad band in the spectrum. **1** and **2** exhibited magnetic moment values of 2.22 and 1.80 BM, respectively, which correspond to one unpaired electron. Complex **3** shows room temperature magnetic moment of 3.47 BM corresponding to three unpaired electrons (one from copper and two from nickel). The most significant frequencies in the IR spectra of **1**, **2**, and **3** are presented in table S2. The broad bands at 3162, 3465, and 3087 cm^{-1} are attributed to ν(OH) of water molecules or ligand for **1**, **2**, and **3**, respectively. The absorption at 3081 cm^{-1} was assigned to ν(NH) of eim in **1**. In the middle energy range, the 2923 and 2932 cm^{-1} absorptions originate from ν(CH) for **1** and **2**, respectively. This peak was not present in **3**'s spectrum. The strong absorptions at 1640, 1633, and 1612 cm^{-1} are due to ν(C=C) + ν(C=N) of ligands for **1**, **2**, and **3**, respectively. In the spectra free H_2pydc, [45] acid disappeared and a new carboxylate band $\nu_s(COO^-)$ appeared at 1360 cm^{-1} for **1**, 1384 cm^{-1} for **2**, and 1361 cm^{-1} for **3**, indicating that the carboxylic group of H_2pydc participates in coordination through deprotonation. Several $\nu_{as}(COO^-)$ strong bands in free H_2pydc are shifted to lower frequencies 1567, 1595, and 1573 cm^{-1} in **1**, **2**, and **3**, respectively. The difference between the asymmetric and symmetric carboxylate stretch ($\Delta = \nu_{as}(COO^-) - \nu_s(COO^-)$) is often used for correlation of infrared spectra with the structures of metal carboxylates [46]. These values are approximately 228 cm^{-1} for monodentate carboxylate [47]. These differences were determined as $\Delta = 207$ cm^{-1} (1567–1360 cm^{-1}, monodentate) for **1**, $\Delta = 211$ cm^{-1} (1595–1384 cm^{-1}, monodentate) for **2**, $\Delta = 212$ cm^{-1} (1573–1361 cm^{-1}, monodentate) for **3**. Absorptions at 575 and 525 cm^{-1} correspond to Cu–O vibration and bands at 455 and 433 cm^{-1} are attributed to Cu–N vibrations of **1** and **2**, respectively. The absorption at 539 cm^{-1} corresponds to M–O vibration and the band at 427 cm^{-1} is attributed to the M–N for **3** (M = Cu(II) or Ni(II)). Chemical structures of the ligands and complexes used in this study are given schemes 1 and 2.

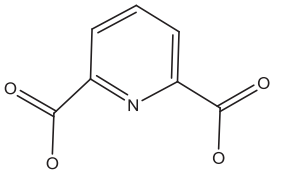

H_2pydc = 2,6-Pyridinedicarboxylic acid

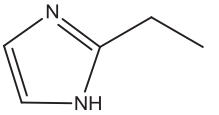

eim = 2-ethylimidazole

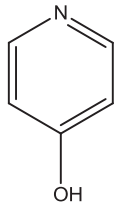

4hp = 4-hydroxypyridine

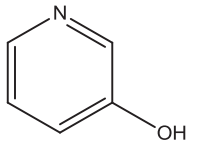

3hp = 3-hydroxypyridine

Scheme 1. Chemical structures of the ligands used in this study.

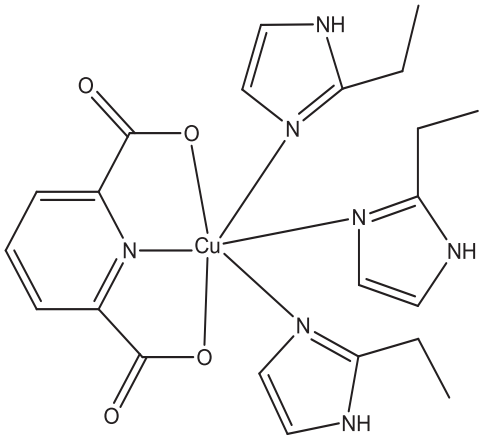

[Cu(pydc)(eim)$_3$]·H_2O (**1**)

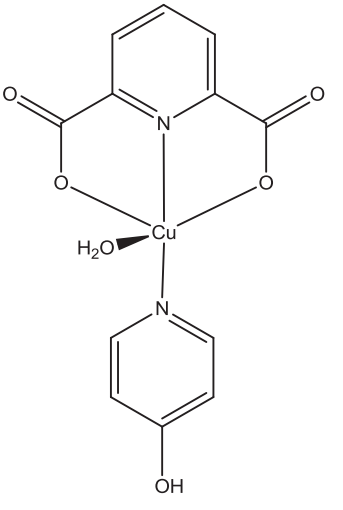

[Cu(pydc)(4hp)(H_2O)] (**2**)

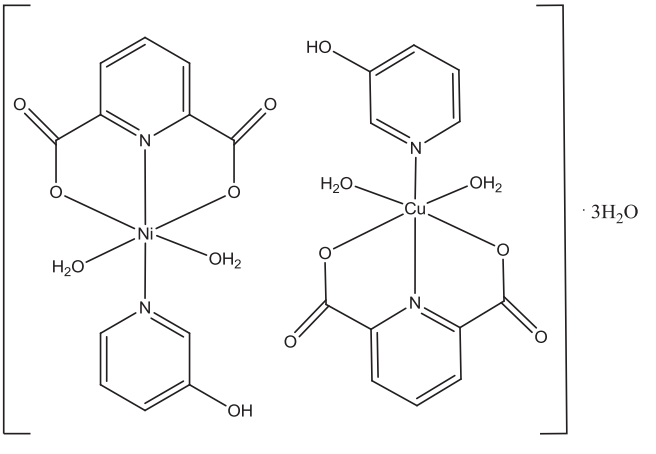

[Ni(pydc)(3hp)(H_2O)$_2$][Cu(pydc)(3hp)(H_2O)$_2$]·3H_2O (**3**)

Scheme 2. Chemical structures of the complexes used in this study.

3.2. *Description of the crystal structures*

3.2.1. [Cu(pydc)(eim)$_3$]·H$_2$O (1). Figure 1 shows the numbering scheme of **1**. Selected bond distances and angles, as well as the data of hydrogen-bonding interactions, are given in table S3. The structural unit is built from one copper(II), three *N*-coordinated 2-ethyl-1H-imidazoles, and one tridentate pydc. The copper(II) ion is chelated by one nitrogen (Cu–N 2.002 Å) and two oxygens from different carboxyl groups of pydc (Cu–O 2.253–2.233 Å), and three nitrogens (Cu–N 2.006, 2.153, 2.124 Å) from three ethylimidazoles. Thus, Cu(II) exhibits distorted octahedral coordination geometry. Among the six coordination sites, four are almost on an equatorial plane (maximum deviation from Cu/O1/O3/N1/N5 mean plane is 0.031 Å for N1) and occupied by nitrogens from pyridine and imidazole; the two sites in the axial position are occupied by another two imidazole molecules (figure 1). The equatorial Cu–N bonds are smaller than the axial Cu–N bonds, similar to the values in the literature for related Cu(II) complexes [18, 48]. The presence of lattice water in the packing of **1** gives a 3-D architecture. All H-bond distances in the range of 2.8–3.3 Å, (table S3) indicate effective O–H···O and N–H···O interactions. The strongest hydrogen bonds are N(4)–H(4A)···O(5) [D···A = 2.800(7) Å] and O(5)-H(5A)···O(2) [D···A = 2.855(7)Å] (figure 2).

3.2.2. [Cu(pydc)(4hp)(H$_2$O)] (2). A perspective view of **2**, together with the atom-numbering scheme, is presented in figure 3, and relevant bond parameters are also summarized in table S4. In mononuclear [Cu(pydc)(4hp)(H$_2$O)], the copper centers are five-coordinate CuO_3N_2 coordination with a distorted square-pyramidal geometry (maximum deviation from Cu/O1/O3/N1/N2 mean plane is 0.186 Å for Cu). The basal positions are occupied by N1 and N2 of the chelating pydc and *pyridine-4-ol* ligand, O1 and O3 of pydc [Cu–N/O

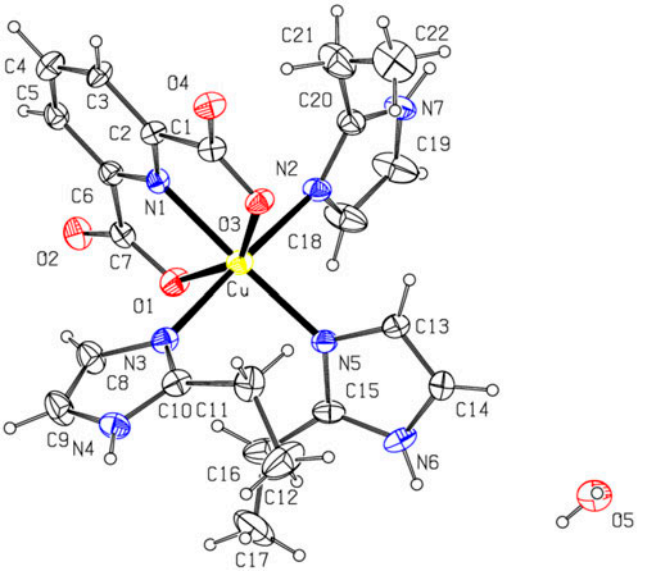

Figure 1. Molecular structure of **1** with atom-labeling scheme. Displacement ellipsoids are present at 40% probability.

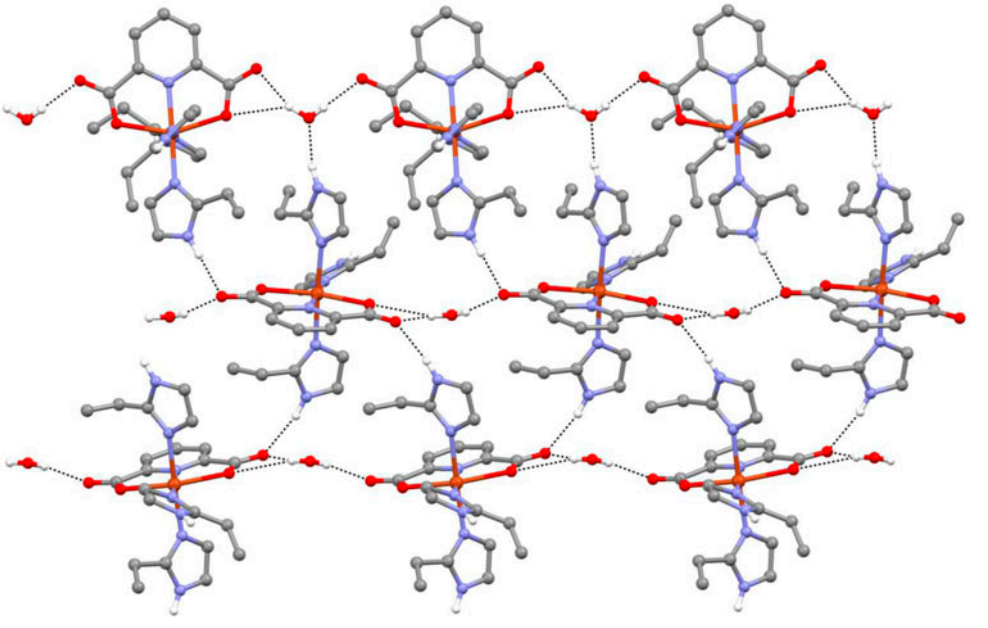

Figure 2. A view of the 2-D hydrogen bonding network of **1**. Hydrogens not involved in hydrogen bonds were omitted for clarity.

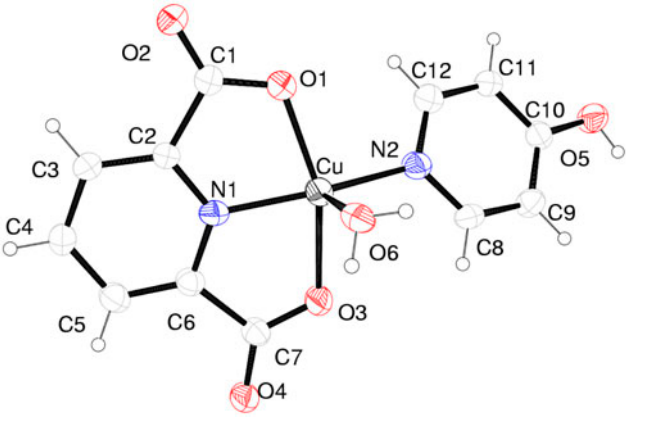

Figure 3. The molecular structure of **2** with atom-labeling scheme. Displacement ellipsoids are present at 40% probability level.

from 1.899(3) to 2.043(4) Å], and O6 of water ligand in the axial position [Cu–O6 2.223(3) Å]. Strong O5–H···O4 (O5···O4 = 2.656 Å) *H* bonds direct the structures into a dimeric form [figure 4(a)]. The intra-dimeric Cu···Cu#1 (#1: $2-x$, $2-y$, $1-z$) distance is 8.072(3)

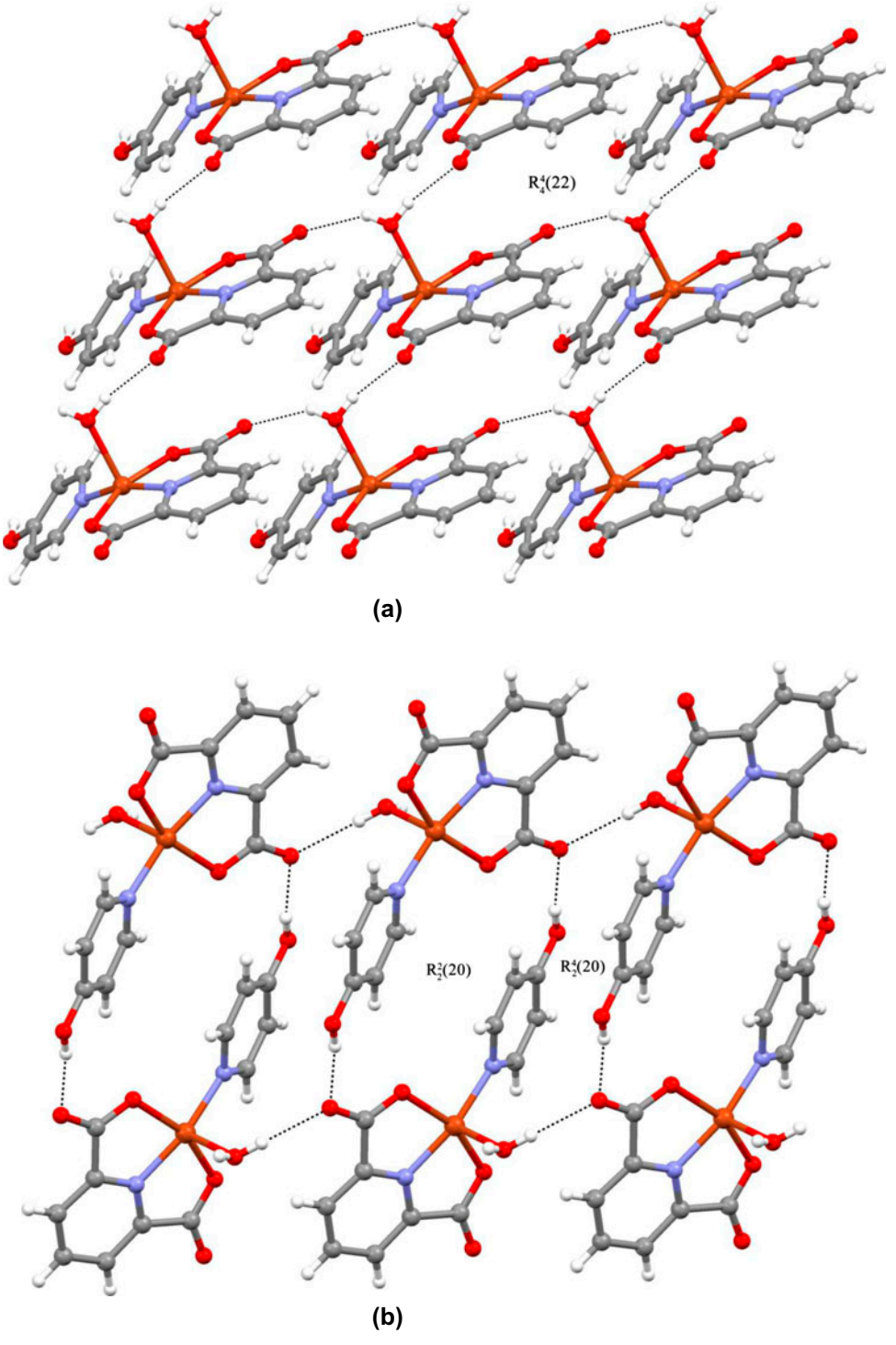

Figure 4. A partial view of the packing of **2**, showing the (a) $R_4^4(22)$, (b) $R_2^2(20)$, and $R_2^4(20)$ ring patterns.

Å, whereas the shortest inter-dimer separation is 6.485(3) Å. Hydrogen bonds between coordinated water and the dimeric neighboring ligands, O3–H3···O5 ($2-x$, $1-y$, $1-z$), form a supramolecular 3-D laminated system oriented along the diagonal axis of the unit cell. As is seen from figure 4(a), hydrogen bonds between the water and carboxylate of pydc constitute a $R_4^4(22)$ ring. It is also found that the carboxylate groups interact with OH groups of OHpy ligands and that exocyclic O of pydc are linked to water ligands by hydrogen bonds, giving $R_2^2(20)$ and $R_2^4(20)$ring motives, respectively [figure 4(b)].

3.2.3. [Ni(pydc)(3hp)(H_2O)$_2$][Cu(pydc)(3hp)(H_2O)$_2$]·3H_2O (3). Complex **3** crystallizes in the monoclinic $P2_1/c$ space group. The asymmetric unit consists of neutral mononuclear complexes [Ni(pydc)(3hp)(H_2O)$_2$], [Cu(pydc)(3hp)(H_2O)$_2$] and three water molecules. A view of the complexes is shown in figure 5. Selected bond distances and angles, as well as data of hydrogen-bonding interactions, are given in table S5. The heteronuclear complex consists of similarly coordinated Cu(II) and Ni(II) units. Each complex is built up from one metal(II), one *N*-coordinated 3-hydroxypyridine, two water ligands, and one tridentate pydc. In the heteronuclear [M(3-hydroxypyridine)(pydc)$_2H_2O$] complexes, the metal centers exhibit six-coordinate MO_4N_2 coordination with a distorted octahedral coordination geometry (maximum deviation from Cu/O3/O4/N3/N4 mean plane is 0.007 Å for N3, for Ni/O10/O11/N1/N2 mean plane is 0.008 Å for Ni). The basal positions are occupied by N1/ N2 and N3/N4 of the chelating pydc and 3-hydroxypyridine, O3/O4 and O10/O11 of pydc; O1/O2 and O8/O9 of water in axial positions. The M(Ni/Cu)–N distances vary from 1.976(2) to 2.003(2) Å, which are typical for a six-coordinate nickel(II) d^8 and copper(II) systems [1, 18]. The M–O distance of 2.068(4)–2252(4) Å lies within the previously reported values ({[Ni(L)(pydc)$_2$]·H_2O}$_n$ (L = 2,5,9,12-tetramethyl-1,4,8,11-tetraazacyclotetradecane) [49, 50]; Ni–O = 2.115(4), 2.086(4) Å, [Ni_2(pydc)$_2$(H_2O)$_5$]·2H_2O [51]; Ni–O = 2.098(3), 2.159(3), 2.164(3), 2.179(3)Å. [Cu(pydc)($C_7H_6N_2$)(H_2O)]·0.75H_2O [52]; Cu–O = 2.001(3), 2.052(3), 2.242(3) Å. The presence of lattice water molecules in **3** gives a 3-D architecture.

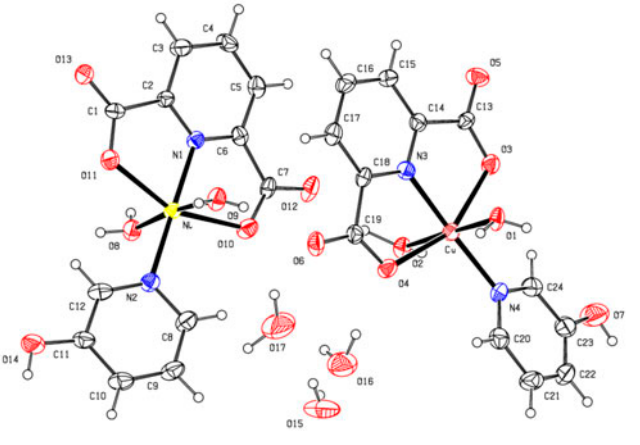

Figure 5. Molecular structure of **3** with atom-labeling scheme. Displacement ellipsoids are present at 40% probability.

All the H-bond distances (table S5) indicate effective O–H···O interactions in a range of 2.628(9)–3.056(8) Å.

Water clusters play a significant role in the stabilization of supramolecular systems in the solid state [53, 54]. The structural determination of water clusters is a key to gain insight into the nature of the hydrogen bond [55, 56]. In **3**, the three lattice waters (O15, O16, and O17) are self-assembled, forming one-dimensional water cluster through hydrogen bonds [figure 6(a)]. The average of O···O distances within 1-D water cluster is 2.96 Å, which is slightly longer than that observed in liquid water (2.85 Å) [57]. The nickel coordinated water (O8) is connected to the 1-D water cluster at 2.805(9) Å. Moreover, the [Ni(pydc)

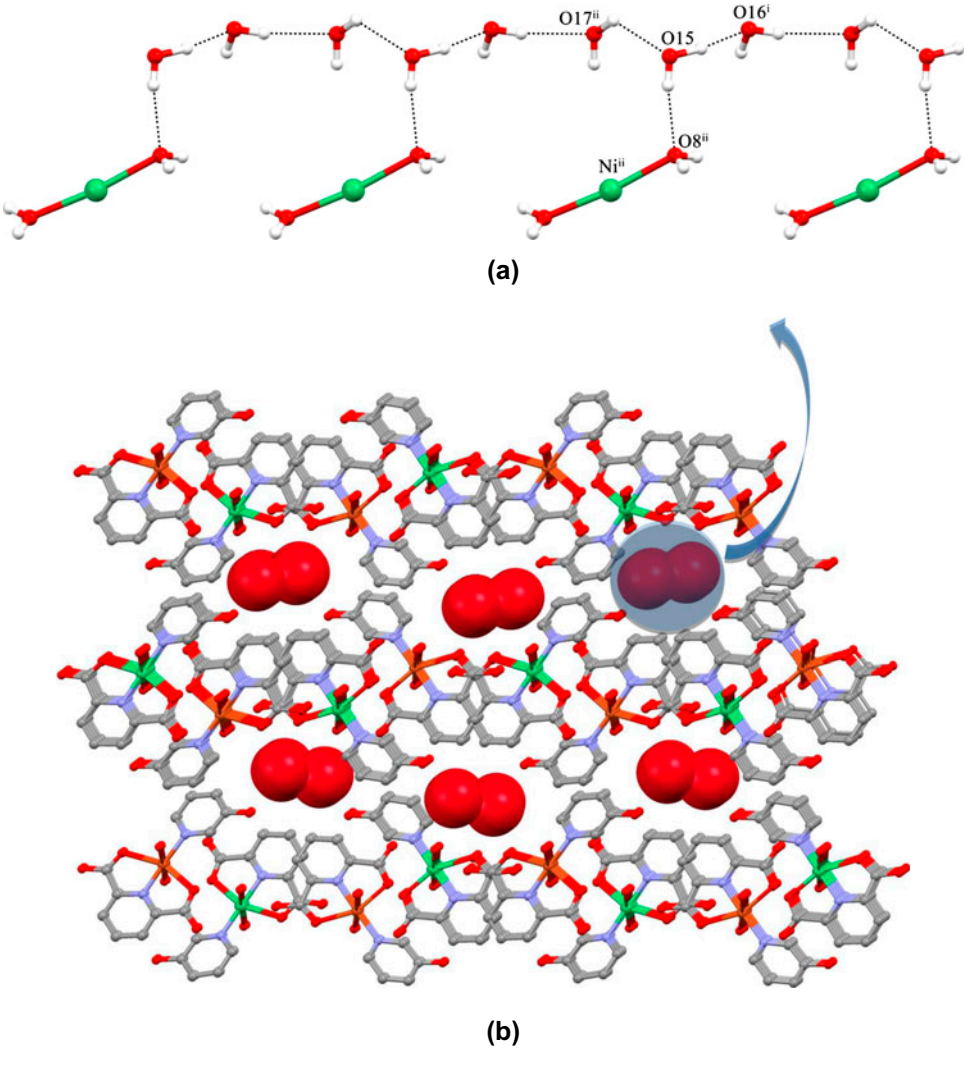

Figure 6. (a) View of a 1-D water cluster and (b) the 3-D supramolecular network of **3**. Hydrogens were omitted for clarity. Symmetry codes: (i) $1-x, -1/2+y, 1/2-z$; (ii) $2-x, -y, 1-z$.

$(3hp)(H_2O)_2]$ and $[Cu(pydc)(3hp)(H_2O)_2]$ complexes are linked by adjacent 1-D water chains to form a 3-D supramolecular network [figures 6(b) and 7].

3.3. *Thermal analysis*

Thermal stabilities of organic [58–60], inorganic [61, 62], and polymer [63, 64] complexes are very important for potential applications.

The TG-DTA and DTG curves of all complexes are given in figure 8. Thermal stabilities of all complexes are similar and decomposition starts at 300, 306, and 300 K respectively. The decomposition of **1** is more complex than **2** and **3**. Decomposition of **1** has 7 consecutive stages and CuO is formed as a residue. The maximum rates of mass loss, as shown in the DTG curve of **1**, are observed at 321, 390, 473, 523, 555, 579, and 671 K, respectively. The decomposition of **2** proceeds with three successive stages. The first corresponds to dehydration of one mole of crystal water; the second stage refers to formation of CuC_2O_4 intermediate product. Finally, the last stage represents formation of CuO residue. Unlike the

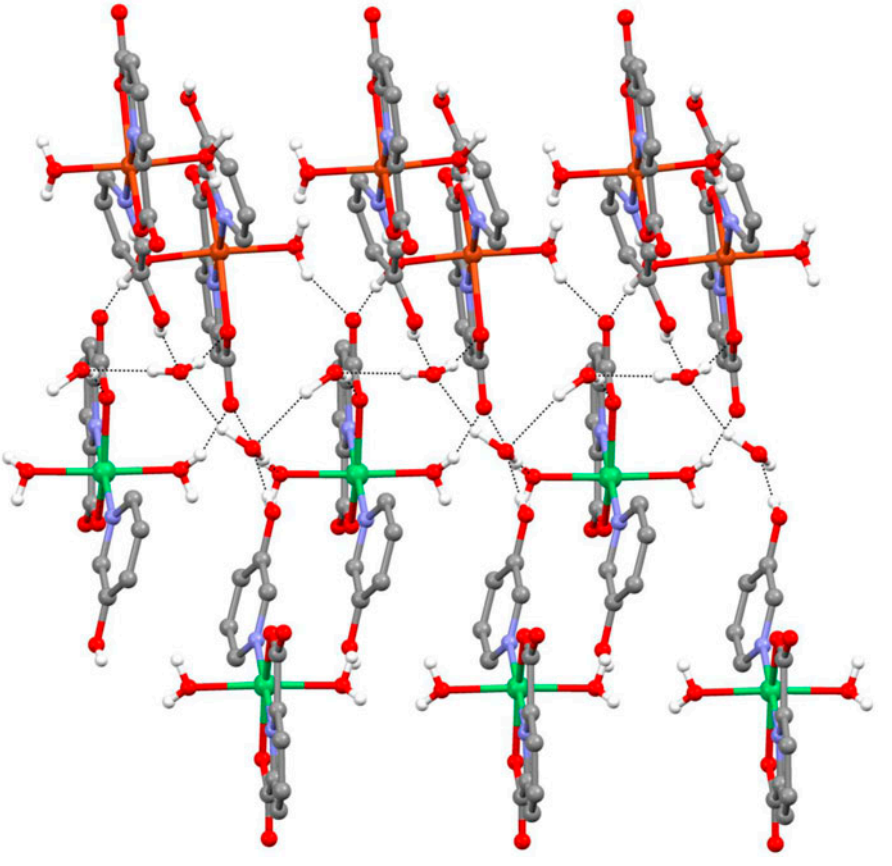

Figure 7. Hydrogen bonding interactions between 1-D water cluster and **3**. Hydrogens not involved in hydrogen bonds were omitted for clarity.

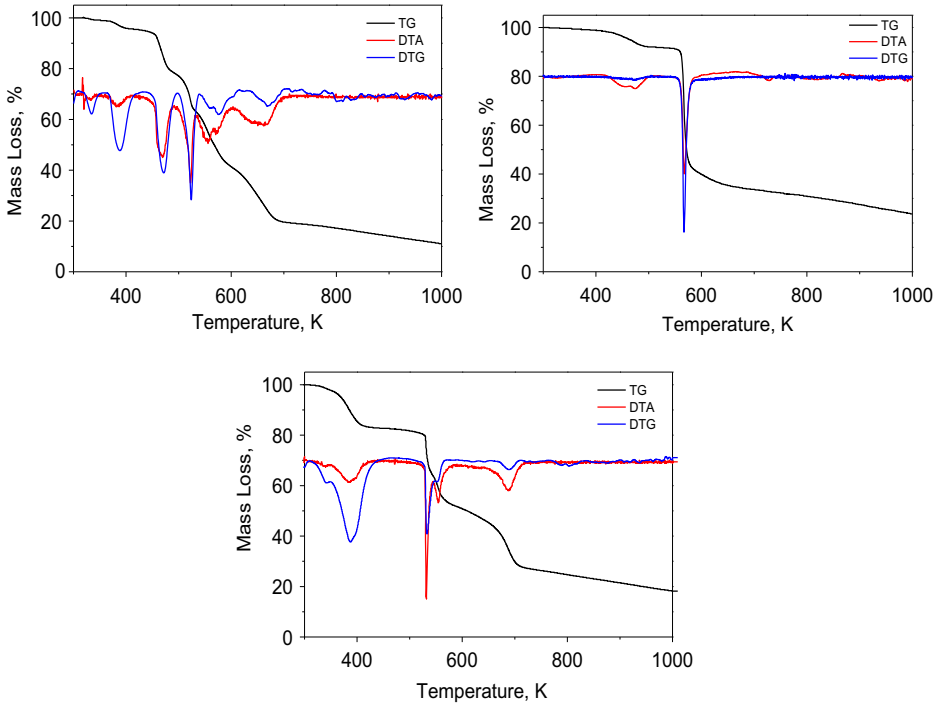

Figure 8. The TG/DTA/DTG curves of **1, 2**, and **3**, respectively.

first two complexes, the decomposition of the complex **3** completes the formation of CuONiO residue. Decomposition occurs in four stages. The total experimental mass loss (80.37%) is compatible with theoretical mass loss (79.58%).

3.4. *Discussion of cytotoxic and anticancer effects of complexes*

The effects of complexes on the proliferation of HT-1080 fibrosarcoma cells were investigated using the quick cell proliferation assay. The cell viability changes depend on the concentrations and type of complexes. Results are shown in figure 10. The complexes inhibited the proliferation of HT-1080 human fibrosarcoma cells in a concentration-dependent manner. Half-maximal inhibitory concentration (IC_{50}) values were determined after 24 h incubation. The complexes were dissolved in WFI. According to the cell proliferation/viability data, **3** was determined to be the most toxic and **1** was the least toxic. Cell membrane damage was also monitored using the LDH leakage assay, because LDH is a stable cytosolic enzyme in normal cells and can leak into the extracellular fluid only after membrane damage. Exposure to complexes (24 h) at 25, 50, and 100 µM doses resulted in LDH release from HT-1080 cells to varying extents (figures 9–13). Treatment using **2** and **3** of 25 µM resulted in a remarkable increase in LDH release. The nuclear morphology of the HT-1080 cells were analyzed using DAPI staining fluorescence microscopy. We observed some

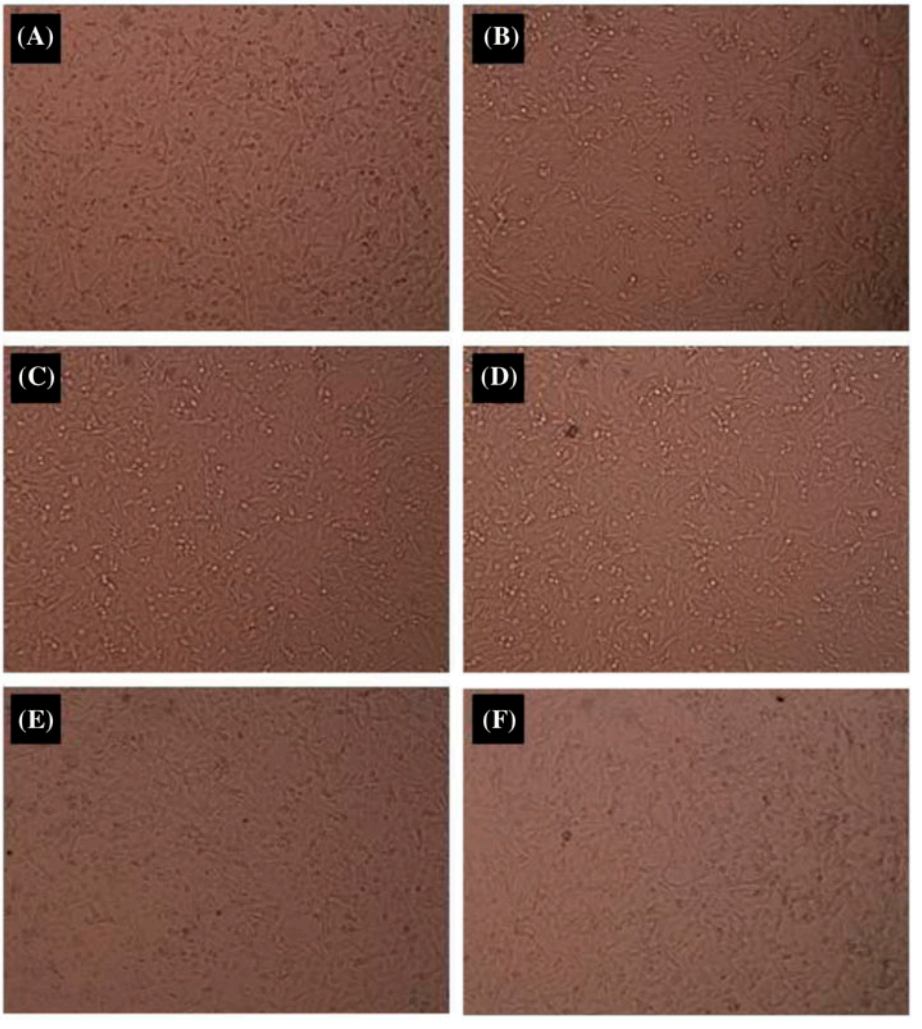

Figure 9. Dose-dependent cell morphology for **1**, **2**, and **3**, in HT-1080 cell line. (**A**), **1** Control, (**B**), **1** 100 μM, (**C**) **3** Control, (**D**) **3** 100 μM, (**E**) **2** Control, and (**F**) **2** 100 μM; 24 h incubation.

pycnotic nuclei, anisonucleosis, and nuclear condensation in cells treated with 100 μM of **3**. This nuclear morphological change precedes chromatin condensation and can be dissociated from many early apoptotic events, such as DNA cleavage and cell shrinkage. The differences in the antiproliferative actions of **1**, **2**, and **3** indicate that the dipicolinate complexes have different antiproliferative activities on fibrosarcoma cells. Targeting apoptosis with the complexes is a promising strategy for cancer drug discovery. The present data will aid in future studies. In investigating the agents that trigger cancer cell death, the sensitivity of tumor cells indicate the success of chemotherapies and the reduced costs of treatment.

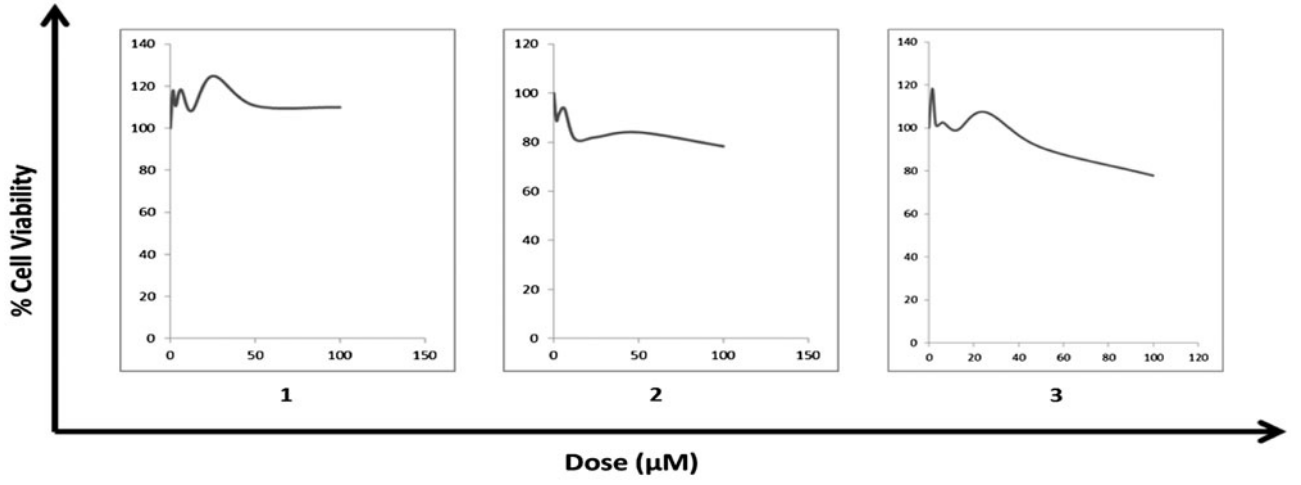

Figure 10. HT-1080 cells were seeded in 96-well microtiter plates. Cells were treated with different concentrations of complexes and incubated for 24 h. WST-1/Electrocoupling solution was added in all control and treatment groups. After 8 h, incubation absorbance values were measured at 420–650 nm reference wavelengths in a microtiter plate reader. The results were presented as percentage of cell viability from that of the respective control samples.

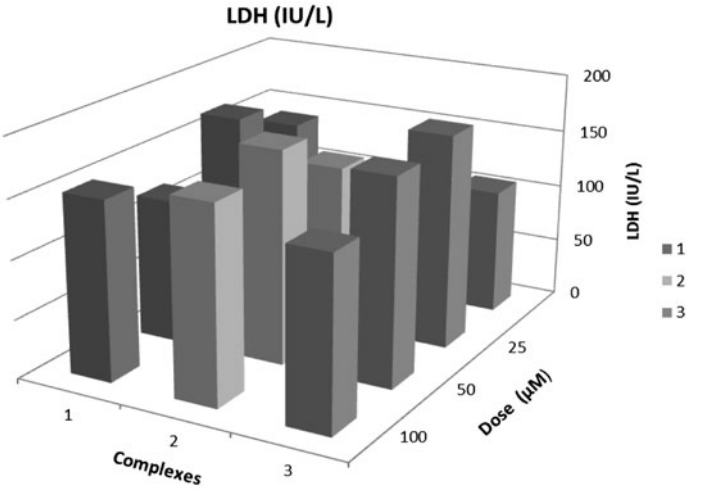

Figure 11. Effect of 1, 2, and 3 exposure on supernatant levels of LDH (IU/L) of HT-1080 cells. Cells were treated with complexes for 24 h in cell culture conditions. Supernatant LDH analysis was carried out using an auto-analyser.

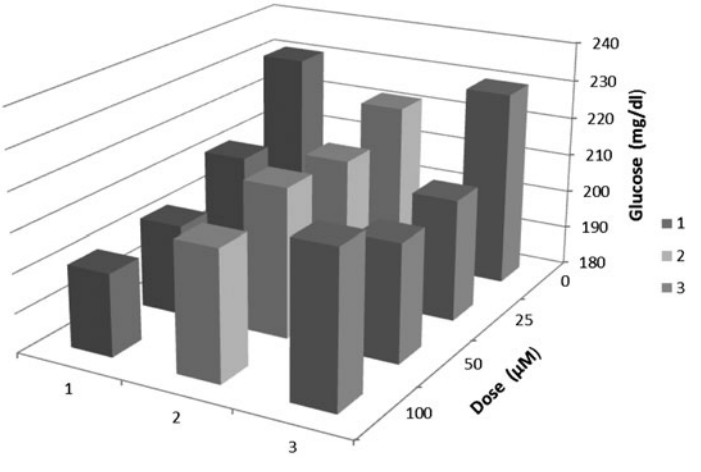

Figure 12. Effect of 1, 2, and 3 exposure on supernatant levels of glucose (mg/dl) levels of HT-1080 cells. Cells were treated with complexes for 24 h in cell culture conditions. Supernatant glucose analysis was carried out using an auto-analyser.

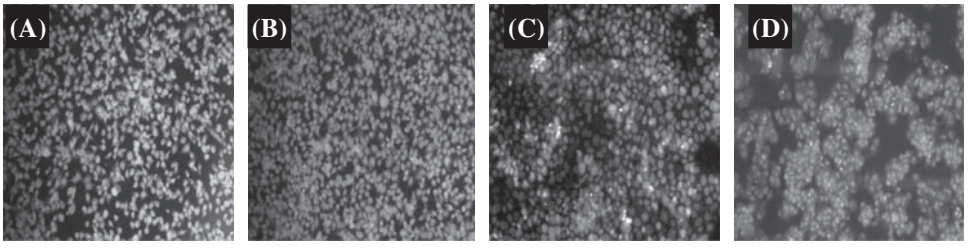

Figure 13. Dose dependent DAPI nuclear staining for **1**, **2**, and **3** in HT-1080 cell line. (**A**) Control, (**B**) **1** (100 μM), (**C**) **2** (100 μM), and (**D**) **3** (100 μM); 24 h incubation.

4. Conclusions

Dipicolinate complexes affect cytotoxicity by 20% on fibrosarcoma cells while copper complexes have weak cytotoxicity on gastrointestinal cell lines [65]. Many articles reported that copper complexes are 10-fold more potent than cisplatin in suppressing the proliferation of human neuroblastoma cells, by arresting the S-phase of cell cycle progression, inducing cellular apoptosis and necrosis, and enhancing the expression of p53 protein [66]. In vitro cytotoxicity assay of $[Cu(Hptc)(Me2bpy)(H_2O)]\cdot 3H_2O$ has considerably higher value than cisplatin (IC50 = 15 μM) against HeLa cell lines, indicating the potential to act as an effective metal-based anticancer agent. Copper (II) complex exhibited effective oxidative DNA cleavage activity in the presence of H_2O_2 [67]. Most of the copper complexes were used either as anticancer agents or they were applied for the treatment of human promyelocytic leukemia cells and other applications for treatment of breast, lung, colon, kidney, pancreatic, and prostate cancer, human squamous cervix carcinoma cells, endometrial and ovarian carcinoma, melanoma-skin, renal carcinoma, non-Hodgkin's lymphoma, human osteogenic sarcoma, malignant melanoma, and mammary gland cancer. Cellular concentrations of copper in tumor cells and tissues should be high enough to promote complex formation. Tumors could be treated with copper ligands alone that would be non-toxic to cells, but could bind to tumor cellular copper, forming potent proteasome inhibitors. The complexes have specific effect, for example, they could induce apoptosis in cancer cells or they are antiproliferative anticancer agents with cytotoxic selectivity [68].

Supplementary material

CCDC-975184, 974852, and 975480 contains the supplementary crystallographic data for **1–3**. These data can be obtained free of charge via http://www.ccdc.cam.ac.uk/conts/retrieving.html, or from the Cambridge Crystallographic Data Center, 12 Union Road, Cambridge CB2 1EZ, UK; Fax: +44 1223 336 033; or e-mail: deposit@ccdc.cam.ac.uk.

References

[1] R. Cini. *Comments Inorg. Chem.*, **22**, 151 (2000).
[2] D. Kovala-Demertzi. *J. Inorg. Biochem.*, **79**, 153 (2000).

[3] D. Kovala-Demertzi, M. Staninska, I. Garcia-Santos, A. Castineiras, M.A. Demertzis. *J. Inorg. Biochem.*, **105**, 1187 (2011).
[4] M. Devereux, D. O'Shea, A. Kellett, M. McCann, M. Walsh, D. Egan, C. Deegan, K. Kędziora, G. Rosair, H. Müller-Bunz. *J. Inorg. Biochem.*, **101**, 881 (2007).
[5] K.M. Vyas, R.N. Jadeja, D. Patel, R.V. Devkar, V.K. Gupta. *Polyhedron*, **65**, 262 (2013).
[6] R.P. Sharma, A. Saini, P. Venugopalan, S. Khullar, S. Mandal. *Polyhedron*, **56**, 34 (2013).
[7] H.H. Hammud, G. Nemer, W. Sawma, J. Touma, P. Barnabe, Y. Bou-Mouglabey, A. Ghannoum, J. El-Hajjar, J. Usta. *Chemico-Biological Interactions*, **173**, 84 (2008).
[8] T. Theophanides, J. Anastassopoulou. *Crit. Rev. Oncol. Hematol.*, **42**, 57 (2002).
[9] T.F. Kagawa, B.H. Geierstanger, A.H. Wang, P.S. Ho. *J. Biol. Chem.*, **266**, 20175 (1991).
[10] J.R.J. Sorenson. *Biology of Copper Complexes*, p. 243, Hunmana Press, New York (1987).
[11] J.R.J. Sorenson. *Prog. Med. Chem.*, **26**, 437 (1989).
[12] J.E. Weder, C.T. Dillon, T.V. Hambley, B.J. Kennedy, P.A. Lay, J.R. Biffin, H.L. Regtop, N.M. Davies. *Coord. Chem. Rev.*, **232**, 95 (2002).
[13] T. Fujimori, S. Yamada, H. Yasui, H. Sakurai, Y. In, T. Ishida. *J. Biol. Inorg. Chem.*, **10**, 831 (2005).
[14] G. Morgant, N.H. Dung, J.C. Daran, B. Viossat, X. Labouze, M. Roch-Arveiller, F.T. Greenaway, W. Cordes, J.R.J. Sorenson. *J. Inorg. Biochem.*, **81**, 11 (2000).
[15] B. Viossat, J.C. Daran, G. Savouret, G. Morgant, F.T. Greenaway, N.H. Dung, V.A. Pham-Tran, J.R.J. Sorenson. *J. Inorg. Biochem.*, **96**, 375 (2003).
[16] P. Lemoine, B. Viossat, G. Morgant, F.T. Greenaway, A. Tomas, N.H. Dung, J.R.J. Sorenson. *J. Inorg. Biochem.*, **89**, 18 (2002).
[17] A.L. Abuhijleh, C. Woods. *Inorg. Chem. Commun.*, **5**, 269 (2002).
[18] S.W. Jin, W.Z. Chen. *Polyhedron*, **26**, 3074 (2007).
[19] S.K. Ghosh, J. Ribas, P.K. Bharadwaj. *CrystEngComm*, **6**, 250 (2004).
[20] X.D. Dong, Z.G. Zhang. *Acta Cryst.*, **E62**, m1841 (2006).
[21] J.C. MacDonald, P.C. Dorrestein, M.M. Pilley, M.M. Foote, J.L. Lundburg, R.W. Henning, A.J. Schultz, J.L. Manson. *J. Am. Chem. Soc.*, **122**, 11692 (2000).
[22] S.K. Ghosh, J. Ribas, P.K. Bharadwaj. *Cryst. Eng. Comm*, **6**, 250 (2004).
[23] L. Mao, Y. Wang, Y. Qi, M. Cao, C. Hu. *J. Mol. Struct.*, **688**, 197 (2004).
[24] M.P. Brandi-Blanco, D. Choquesillo-Lazarte, J.M. González-Pérez, A. Castiñeiras, J. Niclós-Gutiérrez. *Z. Anorg. Allg. Chem.*, **631**, 2081 (2005).
[25] L.C. Nathan, T.D. Mai. *J. Chem. Crystallogr.*, **30**, 509 (2000).
[26] A.R. Parent, S. Vedachalam, C.P. Landee, M.M. Turnbull. *J. Coord. Chem.*, **61**, 93 (2008).
[27] L. Wang, Z. Wang, E. Wang. *J. Coord. Chem.*, **57**, 1353 (2004).
[28] M. Koman, M. Melník. *J. Moncol. Inorg. Chem. Commun.*, **3**, 262 (2000).
[29] N. Okabe, N. Oya. *Acta Cryst.*, **C56**, 305 (2000).
[30] M.V. Kirillova, M.F.C. Guedes da Silva, A.M. Kirillov, J.J.R. Fraústo da Silva, A.J.L. Pombeiro. *Inorg. Chim. Acta*, **360**, 506 (2007).
[31] L. Yang, D.C. Crans, S.M. Miller, A. la Cour, O.P. Anderson, P.M. Kaszynski, M.E. Godzala, L.T.D. Austin, G.R. Willsky. *Inorg. Chem.*, **41**, 4859 (2002).
[32] A.Y. Ali-Mohamed, S.A.W. Al-Arrayed. *Syn. React. Inorg. Met.*, **32**, 1759 (2002).
[33] H.L. Gao, L. Yi, B. Zhao, X.Q. Zhao, P. Cheng, D.Z. Liao, S.P. Yan. *Inorg. Chem.*, **45**, 5980 (2006).
[34] M. Ranjbar, M. Abolghasem, H. Aghabozorg, G.P.A. Yap. *Anal. Sci.*, **18**, 219 (2002).
[35] T.K. Prasad, M.V. Rajasekharan. *Cryst. Growth Des.*, **8**, 1346 (2008).
[36] S.M. Saylor, R.M. Supkowski, R.L. La Duca. *Inorg. Chim. Acta*, **361**, 317 (2008).
[37] A. Moghimi, S. Sheshmani, A. Shokrollahi, M. Shamsipur, G. Kickelbick, H. Aghabozorg. *Z. Anorg. Allg. Chem.*, **631**, 160 (2005).
[38] T.K. Prasad, M.V. Rajasekharan. *Polyhedron*, **26**, 1364 (2007).
[39] X.Z. Sun, M.H. Zeng, B. Wang, B.H. Ye, X.M. Chen. *J. Mol. Struct.*, **828**, 10 (2007).
[40] J. Chakraborty, H. Mayer-Figge, W.S. Sheldrick, P. Banerjee. *Polyhedron*, **25**, 3138 (2006).
[41] C. Sinthuvanich, A.S. Veiga, K. Gupta, D. Gaspar, R. Blumenthal, J.P. Schneider. *J. Am. Chem Soc.*, **134**, 6210 (2012).
[42] F. Martak, T.A. Christanti. *J. Tech. Sci.*, **25**, 13 (2014).
[43] Rigaku/MSC, Inc., 9009 new Trails Drive, The Woodlands, TX.
[44] G.M. Shedrick. *SHELXS97 and SHELXL97, Program for Crystal Structure Solution and Refinement*, University of Göttingen, Germany (1997).
[45] L. Puntus, V. Zolin, V. Kudryashova. *J. Alloy Compd.*, **374**, 330 (2004).
[46] Z. Vargová, V. Zeleòák, I. Císaøová, K. Györyová. *Thermochim. Acta*, **423**, 149 (2004).
[47] K. Nakamoto. *Infrared and Raman Spectra of Inorganic and Coordination Compounds*, 5th Edn, Wiley Interscience, New York (1997).
[48] J.Y. Lu, A.M. Babb. *Inorg. Chem.*, **41**, 1339 (2002).
[49] H.J. Choi, T.S. Lee, M.P. Suh. *Angew. Chem. Int. Ed.*, **38**, 1405 (1999).
[50] K.Y. Choi, H. Ryu, Y.M. Lim, N.D. Sung, U.S. Shin, M. Suh. *Inorg. Chem. Commun.*, **6**, 412 (2003).

[51] Y.H. Wen, Z.J. Li, Y.Y. Qin, Y. Kang, Y.B. Chen, J.K. Cheng, Y.-G. Yao. *Acta Crystallogr.*, **E58**, m762 (2002).
[52] G.Y. Dong, L.H. Fan, L.X. Yang, I.U. Khan. *Acta Cryst.*, **E66**, m532 (2010).
[53] G.P. Yang, J.H. Zhou, Y.Y. Wang, P. Liu, C.C. Shi, A.Y. Fu, Q.Z. Shi. *CrystEngComm*, **13**, 33 (2011).
[54] P. Misra, M. Nayak, P. Lemoine, R. Koner, S. Mohanta. *J. Coord. Chem.*, **61**, 1088 (2008).
[55] G.P. Yang, L. Hou, Y.Y. Wang, Y.N. Zhang, Q.Z. Shi, S.R. Batten. *Cryst. Growth Des.*, **11**, 936 (2011).
[56] M. Brookhart, M.L.H. Green, G. Parkin. *Proc. Natl. Acad. Sci.*, **104**, 6908 (2007).
[57] A.H. NARTEN, W.E. THIESSEN, L. BLUM. *Science*, **217**, 1033 (1982).
[58] H. Deligöz, Ö. Özen, G.K. Çılgı, H. Çetişli. *Thermochim Acta.*, **426**, 33 (2005).
[59] Ö.Ö. Karakuş, G.K. Çilgi, H. Deligöz. *J. Therm. Anal. Calorim.*, **105**, 341 (2011).
[60] A. Saponar, E.J. Popovici, I. Perhaita, G. Nemes, A.I. Cadis. *J. Therm. Anal. Calorim.*, **110**, 349 (2012).
[61] H. Deligöz, Ö. Özen, G.K. Çilgi. *J. Coord. Chem.*, **60**, 73 (2007).
[62] S. Söyleyici, G.K. Çılgı. *J. Therm. Anal. Calorim*, **118**, 705 (2014).
[63] M. Ak, G.K. Çılgı, F.D. Kuru, H. Cetişli. *J. Therm. Anal. Calorim*, **111**, 1627 (2013).
[64] E. Jakab, E. Mészáros, M. Omastová. *J. Therm. Anal. Calorim.*, **88**, 515 (2007).
[65] J. Zhao, K. Peng, Y. Guo, J. Zhang, D. Zhao, S. Chen, J. Hu. *J. Coord. Chem.*, **67**, 2344, (2014).
[66] W.A. Wani, Z. Al-Othman, I. Ali, K. Saleem, M.F. Hsieh. *J. Coord. Chem.*, **67**, 2110 (2014).
[67] C.Z. Xie, M.M. Sun, S.H. Li, X.T. Zhang, X. Qiao, Y. Ouyang, J.Y. Xu. *J. Coord. Chem.*, **66**, 3891 (2013).
[68] D. Krajčiová, M. Melník, E. Havránek, A. Forgácsová, P. Mikuša. *J. Coord. Chem.*, **67**, 1493 (2014).